LANGMUIR Article
Cite This: Langmuir 2019, 35, 6297−6303
pubs.acs.org/Langmuir

Metal Nanoparticle Enhancement of Electron Transfer to Tethered Redox Centers through Self-Assembled Molecular Films

Santiago E. Herrera,[†] Federico G. Davia, Federico J. Williams, and Ernesto J. Calvo*

Departamento de Química Inorgánica, Analítica y Química Física, INQUIMAE-CONICET, Facultad de Ciencias Exactas y Naturales, Universidad de Buenos Aires, Ciudad Universitaria, Pabellón 2, Buenos Aires C1428EHA, Argentina

Supporting Information

ABSTRACT: Metal-nanoparticle-mediated electron transfer (ET) across an insulator thin film containing nanoparticles with attached redox centers was studied using electrochemical impedance spectroscopy. Specifically, a gold spherical microelectrode was modified with 16-amino-1-hexa-decanethiol, creating an insulator film. This was followed by the electrostatic adsorption of gold nanoparticles and the covalent attachment of Os^{2+} redox centers. A variation of the Creager−Wooster method was developed to get quantitative information regarding the ET kinetics of the system. The experimental data obtained from a single measurement was fitted with a model that decouples two or more ET processes with different time constants and considers a Gaussian distribution of tunneling distances. Two parallel ET mechanisms were observed: one in which the electrons flow by tunneling between the surface and the redox couples with a low $k_{ET}^0 = 1.3\ s^{-1}$ and a second one in which an enhancement of the electron transfer is produced due to the presence of the gold nanoparticles with a $k_{ET}^0 = 7 \times 10^4\ s^{-1}$. In this study, we demonstrate that the gold nanoparticle electron transfer enhancement is present only in the local environment of the nanoparticle, showing that the nanoscale architecture is crucial to maximize the enhancement effect.

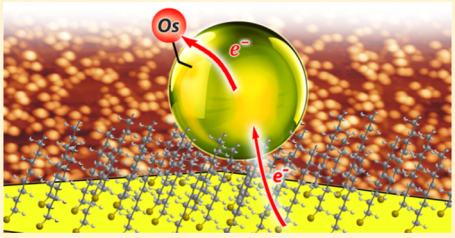

INTRODUCTION

The impressive electron transfer (ET) enhancement by metal nanoparticles (NPs) across an insulating layer was first reported by the groups of Schiffrin[1] and Natan[2] and further studied independently and in great detail by Fermín[3−5] and Gooding.[6−9] The phenomenon is typically observed when electrons are transferred from/to a metal electrode across insulating self-assembled monolayer films modified with metal nanoparticles to/from soluble freely diffusing redox systems. Without the nanoparticles, ET is hindered by the insulating film, and with the nanoparticles, ET is observed with a rate comparable to that of the bare electrode. The metal nanoparticle ET enhancement is also observed when redox centers are covalently attached to the nanoparticles.[10−13] In these studies, ET measurements are carried out using cyclic voltammetry and the Laviron analysis,[14,15] which imposes an upper limit to the ET rate constants, e.g., $k_{ET}^0 = 10^4\ s^{-1}$ for a scan rate of 1200 V s^{-1}.

Ulstrup and Schiffrin[12] suggested a two-step electron transfer mechanism to explain the ET enhancement observed in redox protein/AuNPs and in metal electrode/insulator/metal nanoparticle with covalently attached ferrocene moieties.[16] The two-step mechanism can be rationalized using a model proposed by Chazalviele and Allongue,[17] where AuNPs act as an electron reservoir with a fast metal-electrode-to-nanoparticle electron transfer rate followed by a second ET rate-determining step from the nanoparticle to discrete electronic states in the redox molecule. However, it was recently reported that metal/insulating oxide/metal nanoparticle systems[18,19] show a remarkable electron transfer enhancement by 1.3 nm Pt clusters across insulating gaps as large as 5.7 nm,[19] i.e., larger than those predicted by the model of Chazalviele and Allongue.

In this paper, we report the AuNP electron transfer enhancement using a Au metal electrode modified with a 16-amino-1-hexadecanethiol self-assembled monolayer (SAM) insulating layer. The SAM is further modified with 30 nm AuNPs carrying $Os(bpy)_2PyCH_2NH_2Cl$ redox centers covalently bound by C6 α-lipoic acid, resulting in a Au/C16/AuNP/C6-$Os(bpy)_2PyCH_2NH_2Cl$ structure. However, preparation of this system also results in osmium redox centers directly attached to the C16 SAM. Consequently, two electron-transfer processes with distinct ET rates are observed. The slowest is the electron transfer from the gold electrode to the outer sphere osmium redox couple through the C16 insulating layer and the fastest is the ET enhanced by the AuNP across the C6 linker and the osmium functionality. This system is free of the diffusion limitations present in soluble redox systems as the redox centers are attached to the electrode. Because the osmium complex shows very fast ET kinetics, i.e., $k_{ET}^0 > 10^6\ s^{-1}$,[20] electrochemical impedance over a wide frequency range was employed based on the method reported by Creager and Wooster.[21] To determine the ET rate without AuNPs, the osmium complex was also covalently attached to C6 or C16

Received: January 29, 2019
Revised: April 17, 2019
Published: April 23, 2019

DOI: 10.1021/acs.langmuir.9b00280
Langmuir 2019, 35, 6297−6303

Scheme 1. Step-by-Step Au Surface Modification with 16-Amino-1-hexadecanethiol (16-AHDT), AuNP, Lipoic Acid, and $Os[(bpy)_2(PyCH_2NH_2)Cl]PF_6$

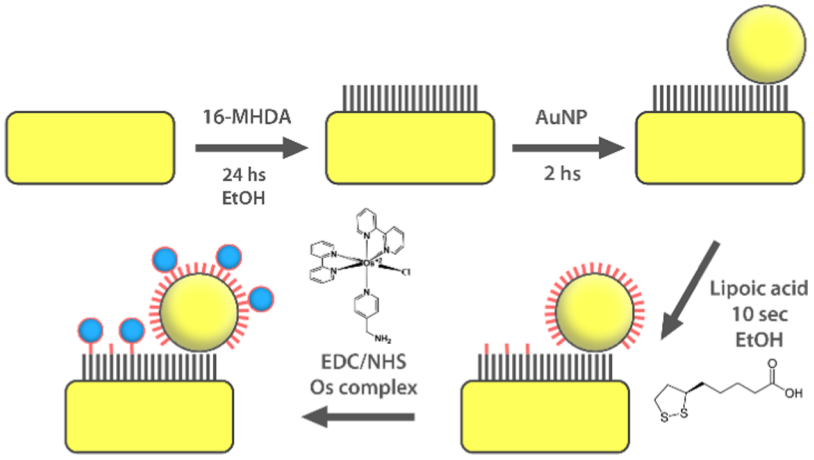

alkanethiol self-assembled monolayers on Au metal electrodes and studied by electrochemical impedance spectroscopy.

The molecular architecture consisting of a gold spherical microelectrode modified with a 16-amino 1-hexadecane-thiol insulating film followed by adsorption of AuNPs and subsequent attachment of Os redox centers was characterized by atomic force microscopy (AFM), scanning tunneling microscopy (STM), and X-ray photoelectron spectroscopy (XPS). The distinctive feature of our approach is that tethered redox centers with very fast kinetics could be measured with an alternating current (ac) technique in a steady-state experiment. We have also introduced in the analysis a Gaussian distribution of tunneling distances to the redox center that allows for a better description of the system.

EXPERIMENTAL SECTION

Materials. 16-Amino-1-hexadecanethiol hydrochloride (16-AHDT) was purchased from Dojindo Chemicals and used as received; α-lipoic acid (LipCOOH), 16-mercaptohexadecanoic acid (16-MHDA), 6-mercapto-hexanoic acid (6-MHA), 1-ethyl-3-(3-dimethyl aminopropyl)-carbodiimide (EDC), *N*-hydroxysuccinimide (NHS), 4-(2-hydroxyethyl)piperazine-1-ethane sulfonic acid (HEPES), potassium nitrate, sodium citrate tribasic dihydrate, chloroauric acid tetrahydrate, and perchloric acid were obtained from Sigma-Aldrich and used as received. The $Os[(bpy)_2(PyCH_2NH_2)Cl]PF_6$ complex was synthesized according to previous reports.[22,23]

Substrates and Surface Preparation. Atomic force microscopy and electrochemical measurements were carried out using a spherical gold microelectrode with a typical diameter of 400 μm prepared by melting the end of a 150 μm diameter gold wire using a Bunsen burner. STM and XPS measurements were carried out on a hydrogen-flame-annealed Au(111) single-crystal electrode (MaTeck, Germany).

Synthesis of Gold Nanoparticles. Citrate-stabilized AuNPs were prepared following the Frens method.[24] Briefly, 50 mL of a 3 mM $HAuCl_4$ aqueous solution was placed on a 100 mL flask connected to a reflux system. The solution was heated until boiling, and 1 mL of a preheated 0.75 M trisodium citrate aqueous solution was added, acting as a reducing and capping agent. After 20 min of reaction, a dark red solution of gold nanoparticles was obtained.

Surface Modification and Redox Probe Binding. The gold surface modification (Scheme 1) started with the self-assembly of the long-chain amino-alkanethiol.

A freshly prepared gold sphere microelectrode was incubated for 24 h in 5 mM 16-amino-1-hexadecanethiol (16-AHDT) in ethanol and then washed with ethanol and Milli-Q water. Then, citrate-stabilized Au nanoparticles were electrostatically adsorbed for 2 h by soaking the electrode in the nanoparticle-containing solution.

After washing with Milli-Q water, the electrode was immersed for 10 s in a 1 M lipoic acid solution in ethanol and washed with ethanol and Milli-Q water following the work of Gooding.[6] The carboxylic acid groups on the AuNP surface were activated by soaking the electrode in a 10 mM EDC + 10 mM NHS aqueous solution for 30 min. After washing with water, the electrode was immersed in a 0.1 μM aqueous solution of $Os[(bpy)_2(PyCH_2NH_2)Cl]$ PF_6 containing 0.1 M KNO_3 in 10 mM HEPES buffer (pH = 7.2) during 4 h to react the $-COOH$ groups of the lipoic acids with the $-NH_2$ groups of the Os complexes. Also, two freshly prepared gold microelectrodes were modified with 6-MHA and 16-MHDA, respectively, by incubation for 24 h in 5 mM ethanol solutions and used as blank without AuNPs. After washing with ethanol and Milli-Q water, the electrodes were activated with EDC and NHS aqueous solution and $Os[(bpy)_2(PyCH_2NH_2)Cl]PF_6$ was attached covalently as described above.

Electrochemical Experiments. Electrochemical experiments were performed with an Autolab V 30 (Eco Chemie, The Netherlands) controlled by NOVA 1.11 software. The potentiostat was equipped with a 750 kHz bandwidth ADC750 fast sampling module and a Scangen analog sweep module. All electrochemical experiments were carried out at room temperature (20 ± 2 °C) in a purpose-built three-electrode glass cell. A Pt counter electrode and a Ag/AgCl, 3 M KCl reference electrode were employed, and all potentials herein are reported with respect to this reference. The surface coverage and electron transfer constant (k_{ET}^0) for modified electroactive surfaces were measured using electrochemical impedance spectroscopy (EIS) by a modification of the ac voltammetry method described by Creager and Wooster.[21] Briefly, the electroactive redox couples were attached to a 400 μm diameter gold spherical microelectrode as described above to minimize the RC time constant by reducing the double layer capacitance. The end of the electrode was submerged in 1 M $HClO_4$ aqueous solution (supporting electrolyte) to reduce the uncompensated resistance. The working Au microsphere electrode was completely immersed with negligible contact to the supporting wire. The electrode potential was controlled between 0.05 V (Os fully reduced) and 0.55 V (Os fully oxidized) in steps of 25 mV starting from 0.05 V. At each potential, a full spectrum of frequencies between 1 Hz and 1 MHz was applied while recording the phase angle ($\varnothing$), and both real (ReZ) and imaginary (ImZ) components of the impedance with a 10 mV peak to peak sinusoidal input signal.

The mechanism of Au nanoparticle-assisted electron transfer (ET) was investigated quantitatively by measuring the electrochemical impedance response of the system depicted in Scheme 1. To decouple

DOI: 10.1021/acs.langmuir.9b00280
Langmuir 2019, 35, 6297−6303

both ET processes and to obtain quantitative information about the system, the equivalent circuits in Scheme 2 were analyzed.

Scheme 2. Randles Equivalent Circuit (a) with a Single Time Constant and (b) with Several Time Constants[25]

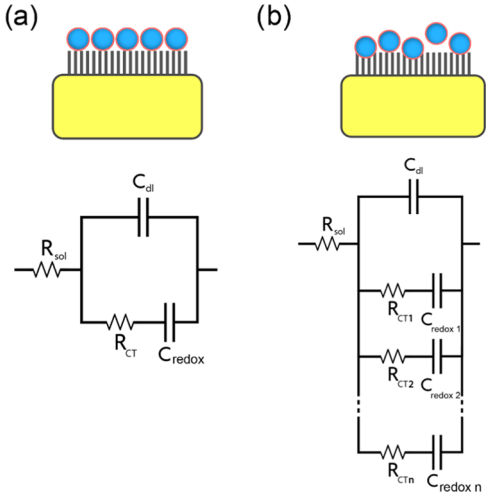

While in Creager's method[21,25] ac voltammetry is employed by ac current ratios $I_{peak}/I_{background}$ vs log(frequency) plot analysis, in this work, steady-state ac impedance was employed (see Experimental Section above). Since E_{ac} is the amplitude of the oscillating potential applied to the circuit, $I_{ac} = \frac{E_{ac}}{Z_{tot}}$ and $\frac{I_{peak}}{I_{background}} = \frac{Z_{tot}^{background}}{Z_{tot}^{peak}}$.

For a single ET process as represented in Scheme 2a, the complex electrochemical cell impedance as a function of the frequency at each potential can be expressed as follows: $Z_{tot} = Z_{R_{sol}} + ((Z_{C_{dl}})^{-1} + (Z_{R_{CT}} + Z_{C_{redox}})^{-1})^{-1}$. Considering that $Z_{R_{sol}} = R_{sol}$ and $Z_{C_i} = -j(\omega C_i)^{-1} = -jX_{C_i}$, the total impedance is as follows: $Z_{tot} = R_{sol} - (jX_{C_{dl}}^{-1} + (R_{CT} + jX_{C_{redox}})^{-1})^{-1}$. Since the experiments were carried out in a high-concentration supporting electrolyte, the solution resistance can be neglected. On the other hand, the charge transfer resistance will depend on the applied potential and, at the formal redox potential ($E = E^{0'}$), the Faradaic charge transfer constant k_{ET} will be maximum and equal to k_{ET}^0 with minimum charge transfer resistance: $R_{CT} = \frac{1}{2C_{redox}k_{ET}}$.

By algebraic operations, we obtain for the imaginary part of the complex impedance

$$\mathrm{Im}(Z_{E=E^{0'}}) = \frac{R_{CT}^2 X_{C_{dl}} + X_{C_{dl}} X_{C_{redox}} (X_{C_{redox}} + X_{C_{dl}})}{-[R_{CT}^2 + (X_{C_{redox}} + X_{C_{dl}})^2]} \quad (1)$$

At potentials far from the Os(III)/Os(II) formal redox potential $E^{0'}$, the background imaginary impedance is determined by the double layer capacitance $\mathrm{Im}(Z_{background}) = -X_{C_{dl}}$. Thus, the ratio $\frac{\mathrm{Im}(Z_{background})}{\mathrm{Im}(Z_{E=E^{0'}})}$ can be expressed in terms of $C_{redox} = \frac{F^2 A \Gamma_{redox}}{RT}$, C_{dl}, and k_{ET}^0 as

$$\frac{\mathrm{Im}(Z_{background})}{\mathrm{Im}(Z_{E=E^{0'}})} = \frac{R_{CT}^2 + (X_{C_{redox}} + X_{C_{dl}})^2}{R_{CT}^2 + X_{C_{redox}}(X_{C_{redox}} + X_{C_{dl}})} = \frac{\omega^2/4k_{ET}^{0\,2} + \left(1 + \frac{C_{redox}}{C_{DL}}\right)^2}{\omega^2/4k_{ET}^{0\,2} + \left(1 + \frac{C_{redox}}{C_{DL}}\right)} \quad (2)$$

Since very small differences in tunneling distances may bring about large differences in the tunneling current, we have further refined the Randles analysis. If the circuit is composed of a large-enough number of RC parallels as depicted in Scheme 2b, the impedance response can be obtained considering a continuous distribution of kinetic constants $\theta(k_{ET})$. By assuming a Gaussian distribution of ET distances, we obtained a distribution of ET rate constants as described elsewhere[26]

$$\theta(k_{ET}) = a \cdot \sum x_i \cdot e^{-1/2 \cdot \beta^2 \sigma^2 \cdot [\ln(k_{ET}/k_{ET}^0)]^2} \quad (3)$$

with "a" the normalization factor, x_i the fraction of the population "i" relative to the total redox species adsorbed, and σ the Gaussian standard deviation. The Gaussian distribution of redox rate constants[25,27] or electrode potentials[28−30] has been previously reported.

Consequently, the imaginary impedance ratio in eq 2 becomes

$$\frac{\mathrm{Im}(Z_{background})}{\mathrm{Im}(Z_{E=E^{0'}})} = \frac{\left(\frac{C_{dl}}{C_{redox}} \cdot \omega + B(\omega)\right)^2 + A(\omega)^2}{\frac{C_{dl}}{C_{redox}} \cdot \omega \cdot \left(\frac{C_{dl}}{C_{AD}} \cdot \omega + B(\omega)\right)} \quad (4)$$

where the integrals $A = \int_0^{+\infty} \frac{\theta(k_{ET})}{2 \cdot k_{ET}\left(\frac{1}{4k_{ET}^2} + \frac{1}{\omega^2}\right)} dk_{ET}$ and $B = \int_0^{+\infty} \frac{\theta(k_{ET})}{\omega\left(\frac{1}{4k_{ET}^2} + \frac{1}{\omega^2}\right)} dk_{ET}$ can be solved numerically to fit the experimental data.

Atomic Force Microscopy (AFM). The gold microelectrode surface was scanned by AFM (EC-AFM, Agilent 5500 AFM/SPM) in tapping mode using triangular silicon tip PointProbe Plus (PPP-NCL, Nanosensors) with a typical resonance frequency of 160 kHz. The gold microsphere was placed over a soft substrate, and the tip was aligned several times until minimal drift was detected after approaching. Image analysis was performed with Gwyddion 2.5 software (http://gwyddion.net/).

Scanning Tunneling Microscopy (STM). Air condition STM measurements were carried out using an Agilent 5500 AFM/SPM in constant current mode. Tungsten tips were made by electrochemical etching in 2 M KOH; cleaned with concentrated hydrofluoric acid, water, and acetone; and used immediately.

Photoelectron Spectroscopy Measurements (XPS). XPS measurements were conducted in an ultrahigh vacuum chamber with a base pressure of 5×10^{-10} mbar, using a 150 mm hemispherical SPECS electron energy analyzer and a monochromatic Al Kα X-ray source. The reported binding energies were referenced to the Fermi edge of Au(111) at EB = 0 eV. N 1s, Os 4f, and C 1s atomic ratios were calculated from the integrated intensities of core levels after instrumental and photoionization cross-section corrections.

RESULTS AND DISCUSSION

Gold Nanoparticles Containing Electroactive Surface Species. First, the surface of a modified gold microsphere (400 μm diameter) with a thick insulator film of 16-amino-1-hexadecanethiol (16-AHDT) was characterized by X-ray photoelectron spectroscopy (XPS). Marmisollé et al. showed that the self-assembly of 16-AHDT molecules creates a highly compact two-dimensional (2D) structure, stabilized by van der Waal forces between long alkyl chains with low water molecule penetration.[31] XPS measurements of 16-AHDT-modified gold electrodes (see Supporting Information (SI)) have shown that the terminal amines were partially protonated, making the surface susceptible for adsorption of negatively charged species.

Negatively charged Au nanoparticles (AuNPs) were subsequently electrostatically adsorbed on the self-assembled monolayer (SAM). Figure 1 shows an atomic force microscopy (AFM) topography image of the gold microsphere modified with 16-MHDT and AuNPs. Height profiles performed on the

DOI: 10.1021/acs.langmuir.9b00280
Langmuir 2019, 35, 6297−6303

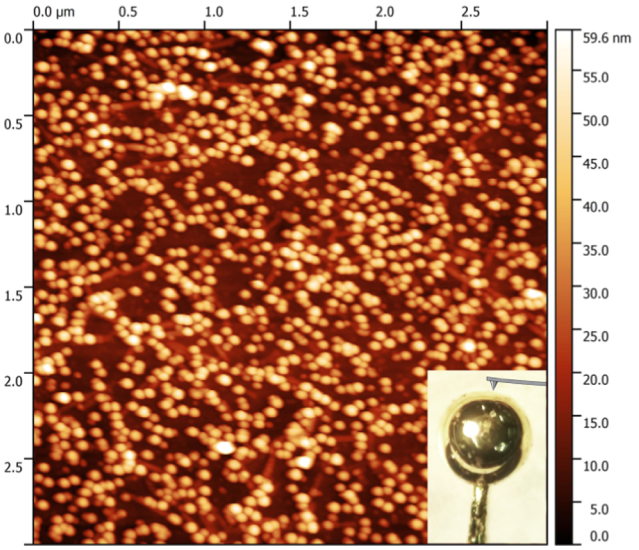

Figure 1. Tapping mode AFM topography image of a gold microsphere modified with 16-AHDT followed by electrostatic adsorption of 30 nm Au nanoparticles. t_{ads} = 2 h.

AFM images indicated an average particle diameter of 30 ± 2 nm. According to the Chazalviel–Allongue theory,[17] the ET enhancement by AuNPs can only be observed for a given range of particle diameter and tunneling barrier height.[17] In the case of a 16 methylene units tunneling barrier, the minimum AuNP diameter necessary to produce the ET enhancement is about 2.5 nm. Thus, a particle with 30 nm diameter over a 16-AHDT SAM should give high-enough Au–AuNP exchange current density to produce the ET enhancement effect.

Reports by Fermín and Gooding have demonstrated that a particle surface coverage of at least 2×10^9 AuNPs cm^{-2} is required to observe ET enhancement for the case of redox couples in solution.[32,33]

The analysis of AFM images over a large number of particles yielded a surface coverage of AuNPs $\Gamma_{AuNP} = 1.4 \pm 0.3 \times 10^{10}$ cm^{-2} on the Au microspheres. This is high enough to observe the AuNP ET enhancement effect.

From the AFM image in Figure 1, it can be observed that AuNPs aggregate in 2D clusters with minimal *z*-overlapping. Hence, the surface clustering produces NP-free zones with areas of approximately 0.05 μm^2.

In addition to the AFM examination, scanning tunneling microscopy (STM) measurements were conducted in air over the surface of the electrode before and after modification with AuNPs (Figure S2 in SI). The images showed a flat topography before and after modification with AuNPs, demonstrating that the STM tip buries into the SAM, exchanging electrons directly from the gold surface. Similar experiments were conducted using different length alkanethiols (C2, C6, C8, and C11), detecting short circuit only for the case of C2 and C6. This result indicates that the particles were placed on top of the SAM without surface contact, consistent with a compact 16-AHDT molecular self-assembled film.

As depicted in Scheme 1, the next step was exposure of the AuNP/C16/Au surface to a solution of α-lipoic acid. Exchange of citrate molecules on the NPs by the carboxylic acid-terminated thiol creates anchoring sites for the Os redox couples. Displacement of citrate on the AuNP surface was achieved by a 10 s short exposure in a concentrated ethanol solution of α-lipoic acid, as reported by Gooding et al.[6] In this step, nonspecific adsorption of thiols may occur over surface regions with no AuNPs by electrostatic interactions between NH_2 and COOH groups. XPS measurements showed that after α-lipoic acid treatment, the N 1s intensity remains almost constant, indicating that no displacement of 16-MHDT occurs during this step (Figure S3 in SI).

The covalent binding of $Os[(bpy)_2(PyCH_2NH_2)Cl]PF_6$ redox complexes was carried out by formation of an amide bond between the terminal carboxylate of α-lipoic acid and the amine group of the Os complex. This reaction was conducted in aqueous solution by employing EDC/NHS as activator and coupling agents.[34] After redox couple modification, the XPS showed the typical Os 4f doublet signal with peaks at 51.3 eV (Os $4f_{7/2}$) and 54.1 eV (Os $4f_{5/2}$) corresponding to Os(II) (see SI).[34]

Electron Transfer Kinetics. First, we examined the electron transfer of soluble freely diffusing 3 mM $[Ru(NH_3)_6]^{3+}$ complexes at the Au/16-AHDT/AuNP surface structure by cyclic voltammetry using a flat Au electrode (see Figure S1 in SI). Without the NPs, the 16-AHDT SAM blocked completely the electron transfer reaction and only double layer charging current was observed, which shows that no pinholes are apparent in the C16 self-assembled monolayer on Au. In agreement with previous reports, adsorption of AuNPs onto the long-chain alkanethiol SAM resulted in electron transfer to the $[Ru(NH_3)_6]^{3+}$, as shown by voltammetry.

Electron transfer kinetics of the tethered osmium molecules was investigated by electrochemical impedance spectroscopy (EIS), applying a spectrum of frequencies to the sample at each fixed applied potential (*E*). This steady-state experiment was repeated for different potentials, in the 0.05–0.55 V range. Figure 2 depicts the EIS spectra by plotting the inverse of the imaginary impedance at each electrode potential, Im(*Z*(*E*)), vs the electrode potential for different frequencies between 500 kHz and 0.1 Hz. Since the values of 1/Im(*Z*(*E*)) span over a very wide range, the data in Figure 2 were normalized by the background imaginary impedance Im($Z_{backbround}$) far from the Os(III)/Os(II) formal redox potential after correcting the base line.

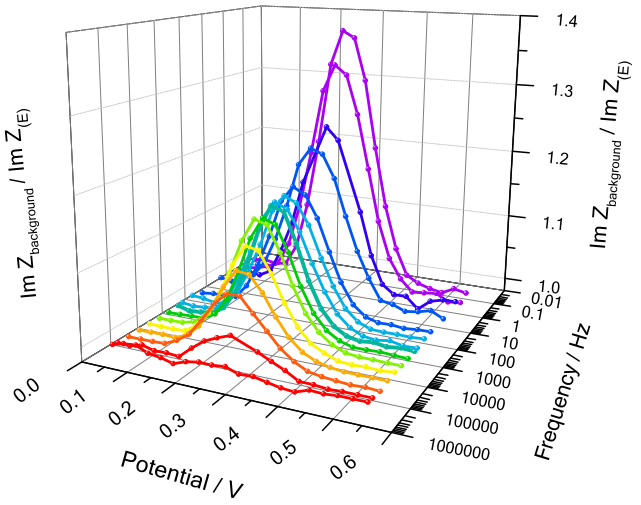

Figure 2. Plot of $ImZ_{background}/ImZ(E)$ vs applied potential at different frequencies from electrochemical impedance spectroscopy measurements for the system Au/AHDT/AuNP/LipCOOH/Os.

DOI: 10.1021/acs.langmuir.9b00280
Langmuir 2019, 35, 6297–6303

At high frequencies, the peak centered at $E^{0'}$ drops to an almost constant value; thus, for frequencies much larger than the ET kinetic constant, $k_{ET}{}^0$, the ac current flows mainly through the double layer. As the frequency decreases, a peak at $E^{0'}$ is observed, which corresponds to the electron transfer to the osmium redox molecules. At frequencies close to 1 kHz, the height of the redox peak becomes independent of the applied frequency, while at lower frequencies, in the 10−0.1 Hz range, the peak height increases again and reaches a new constant value corresponding to a second and slower ET process. Notice that both processes show a peak centered at $E^{0'}$ corresponding to the Os(III)/Os(II) electron transfer reaction; thus, the Os redox centers can exchange electrons by two parallel mechanisms.

At the Os(III)/Os(II) formal redox potential, $E^{0''}$, the plots of $\mathrm{Im}Z_{backound}/\mathrm{Im}Z(E)$ in Figure 2 have a maximum, which is determined by the electron transfer rate constant, $k_{ET}{}^0$, the double layer capacitance C_{dl}, and redox capacitances $C_{redox} = \frac{F^2 A \Gamma_{redox}}{RT}$.

Furthermore, a plot of $\mathrm{Im}Z_{background}/\mathrm{Im}Z_{E = E^{0'}}$ vs the logarithm of the perturbing frequency in a single experiment exhibits two time constants over more than 4 orders of magnitude apart as shown in Figure 3, top panel.

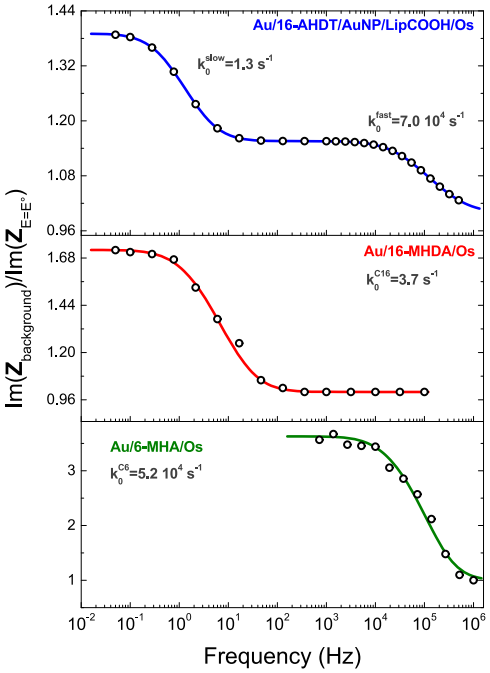

Figure 3. Imaginary impedance ratio as a function of frequency at $E^0_{Os^{3+}/Os^{2+}}$ (circles) and the corresponding fitting to eq 4 (solid line). Os redox molecules anchored on top of AuNP (Au/16-AHDT/AuNP/LipCOOH/Os) (top panel). Os molecules covalently attached to self-assembled monolayers of 16-mercaptohexadecanoic acid (Au/16-MHDA/Os) (middle panel) and 6-mer-capto hexanoic acid (Au/6-MHA/Os) (bottom panel).

Fitting the data assuming a Gaussian distribution of ET distances results in $k_{ET}{}^0(1) = 7.5 \times 10^4$ s^{-1} for the fast process and $k_{ET}{}^0(2) = 1.3$ s^{-1} for the slow ET process, while $C_{dl} = 1.8$ μF and $C_{redox} = 0.7$ μF ($\Gamma_{Os} = 3.7 \times 10^{-11}$ mol cm^{-2}). For comparison, the middle and bottom panels in Figure 3 show reference experiments without AuNPs using short- (C6) and long (C16)-chain alkanethiols, respectively. For Au/16-MHDA/Os, we obtained $k_{ET}{}^0 = 3.7$ s^{-1} ($\Gamma_{Os} = 4.4 \times 10^{-13}$ mol cm^{-2} and $C_{dl} = 0.011$ μF), and for Au/6-MHA/Os, $k_{ET}{}^0 = 5.2 \times 10^4$ s^{-1} ($\Gamma_{Os} = 2.8 \times 10^{-12}$ mol cm^{-2} and $C_{dl} = 0.017$ μF). These values are similar to previously reported data for the same osmium complex tethered by alkanethiols of different lengths.[20]

A comparison of the fast electron transfer rate enhanced by AuNPs with that for C16 without AuNPs yields a remarkable enhancement factor of 1.9×10^4. On the other hand, the electron transfer rate enhanced by AuNPs is very similar to that for C6 alkanethiol, 5.2×10^4 s^{-1}, which suggests that the limiting electron transfer rate in the two-step mechanism is the transfer from the AuNP to the osmium functionality by electron tunneling through the C6 α-lipoic acid linker.

This result is consistent with the mechanism of Chazalviel and Allongue,[17] who considered that the total ET between the electrode and the redox couple can be explained in terms of a two-step ET process: In the first step, the electrons are exchanged across the Au−AuNP gap with a high current density due to the large number of electronic states in the AuNP. In the second step, however, the electron transfer between the AuNP and the redox molecule takes place by the exponential tunneling dependence on distance

$$k_{ET} = k_{ET}^0 e^{-\beta(r-r_0)} \quad (5)$$

with $\beta \sim 1$ Å^{-1} and $d = r - r_0$ is the distance of the redox molecule with respect to the AuNP.[35]

In the Chazalviel and Allongue paper,[17] the authors have considered the reorganization energy for the first step as the electrical work to charge the spherical Au nanoparticle and concluded that the ratio of exchange current densities for both steps could be as large as 10^{12} depending on the AuNP size. Thus, the electron tunneling from the AuNP and the discrete electronic levels in the Os complex should be the rate-determining step for the overall process.

Figure 4 depicts the two weighed Gaussian distributions θ_1 and θ_2 of ET rate constants obtained from the best fit of data in Figure 3, top panel, to eq 4. The total redox osmium molecules surface coverage is $\Gamma_{Os} = 3.7 \times 10^{-11}$ mol cm^{-2}, 40% (1.5×10^{-11} mol cm^{-2}) of which corresponds to the fast electron transfer process mediated by the AuNPs and 60% (2.2×10^{-11} mol cm^{-2}) to the slow electron transfer pathway.

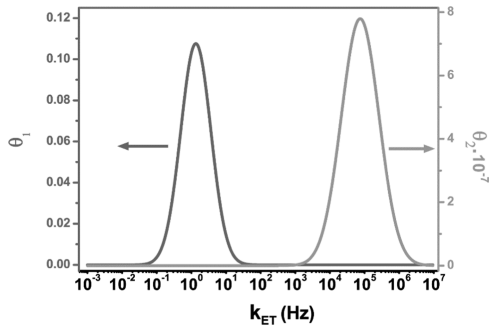

Figure 4. Electron transfer rate constant distributions obtained from the fitting of the experimental data with the heterogeneous Randles equivalent circuit (eq 4) for Au/AHDT/AuNP/LipCOOH/Os. Distribution 1: left axis, slow ET process and distribution 2: right axis, fast ET process. As the area of each curve is equal to 1, a factor of 1×10^{-7} was applied to the right vertical scale for direct visual comparison.

DOI: 10.1021/acs.langmuir.9b00280
Langmuir 2019, 35, 6297−6303

Using a mean molecular diameter for the Os complex of 1.3 nm[34] (molecule projected area, 1.327×10^{-14} cm^2) and the total Os coverage, we estimate a 30% total osmium coverage, with 18% contribution of the slow process and 12% of the fast ET.

While the k_{ET} peak widths in Figure 4 appear to be not significantly different, the logarithmic scale indicates that the fast process has a larger half-peak width with respect to the slow process. As the k_{ET} can be correlated to a tunneling distance (eq 5), a plot of each Gaussian distribution in the tunneling distance space was obtained as depicted in Figure S4 (SI). By analyzing the distance distributions of each ET process, an important difference is observed with a larger Gaussian peak width for the fast ET process and a narrow distribution for the slow ET process. This result is consistent with a highly packed SAM for the C16 alkanethiol and a more disordered SAM for the shorter C6 lipoic acid on the AuNPs, also showing the added value of the Gaussian distance distribution model. The half-width at full maximum for systems C6 and C16 without nanoparticles (6-MHA and 16-MHDA) resulted from the Gaussian distance distributions $FWHM_{C6}$ = 0.330 nm and $FWHM_{C16}$ = 0.223 nm, respectively, while for the NP system, the values obtained were $FWHM_{\theta 2}$ = 0.500 nm for the fast and $FWHM_{\theta 1}$ = 0.309 nm for the slow process.

The $FWHM_{\theta 2} > FWHM_{C6}$ and $FWHM_{\theta 1} > FWHM_{C16}$; therefore, for the same alkanethiol length, the system on AuNP/LipCOOH/Os is more disordered than that for the alkanethiol on a flat gold surface.

CONCLUSIONS

In this work, we have measured the electron transfer rates from a gold electrode to a covalently bound Os bipyridine probe across a long distance given by 16 methylene groups of the 16-amino-1-hexadecane-thiol self-assembled monolayer by ac impedance spectroscopy. Adsorption of 30 nm gold nanoparticles (AuNPs) on the C16 SAM with the osmium centers covalently attached to the AuNPs with a C6 linker has shown a remarkable enhancement with $k_{ET}^0 = 7 \times 10^4$ s^{-1} with respect to 3.7 s^{-1} for the redox centers covalently attached directly to the C16 SAM. This result is consistent with a two-step model proposed by Chazalviel and Allongue with the electron transfer from the AuNP to the osmium molecule as the rate-determining step since the observed $k_{ET}^0 = 7 \times 10^4$ s^{-1} rate constant is comparable to that measured for the osmium centers covalently attached directly to C6 alkanethiol, $k_{ET}^0 = 5.2 \times 10^4$ s^{-1}. The ET rate constants were obtained by fitting the experimental data with a model that introduces a Gaussian distribution of tunneling distances between the AuNP and the redox Os molecule, which also gives a better picture of the molecular surface organization.

It has also been shown that using a fast redox probe tethered to AuNPs faster ET kinetics between the nanoparticles and the molecular redox states can be measured when compared with soluble diffusing redox couples. In a single experiment, two ET processes over 4 orders of magnitude apart could be measured simultaneously, which corresponds to tunneling across C16-SAM/Os and the enhanced transfer by C16-SAM-AuMNP/Os, respectively. This suggests that the ET enhancement effect takes place in the local surroundings of the nanoparticle.

ASSOCIATED CONTENT

Supporting Information

The Supporting Information is available free of charge on the ACS Publications website at DOI: 10.1021/acs.langmuir.9b00280.

Cyclic voltammetry of soluble redox couple; air-STM topography images of Au(111) modified with 16-AHDT and Au(111) modified with 16-AHDT and AuNP; N, Os, and C XPS spectra corresponding to different stages during the functionalization; derivation of Gaussian distribution of ET rate constants; and distributions $\theta 1$ and $\theta 2$ for the system Au/AHDT/AuNP/LipCOOH/Os adapted to the tunneling distance space (PDF)

AUTHOR INFORMATION

Corresponding Author

*(E.J.C.) E-mail: calvo@qi.fcen.uba.ar. Phone: +54 911 4146 2345.

ORCID

Federico J. Williams: 0000-0002-6194-2734

Ernesto J. Calvo: 0000-0003-0397-2406

Present Address

†Instituto de Investigaciones Fisicoquímicas Teóricas y Aplicadas (INIFTA), Facultad de Ciencias Exactas, Universidad Nacional de La Plata—CONICET—Sucursal 4 Casilla de Correo 16, 1900 La Plata, Argentina (S.E.H.).

Author Contributions

All authors have given approval to the final version of the manuscript and have contributed equally.

Notes

The authors declare no competing financial interest.

ACKNOWLEDGMENTS

The authors acknowledge financial support from CONICET, ANCPCyT PICT 2016-4380, and the University of Buenos Aires. E.J.C. and F.J.W. are research fellows of CONICET. S.E.H. and F.G.D. acknowledge doctoral scholarships from CONICET.

ABBREVIATIONS

SAM, self-assembled monolayer; AuNP, gold nanoparticles; ET, electron transfer; AFM, atomic force microscopy; STM, scanning tunneling microscopy; XPS, X-ray photoelectron spectroscopy; EIS, electrochemical impedance spectroscopy; 16-AHDT, 16-amino-1-hexadecanethiol hydrochloride; 16-MHDA, 16-mercaptohexadecanoic acid; 6-MHA, 6-mercaptohexanoic acid; EDC, 1-ethyl-3-(3-dimethyl amino propyl)-carbodiimide; NHS, *N*-hydroxysuccinimide; HEPES, 4-(2-hydroxyethyl)piperazine-1-ethane sulfonic acid

REFERENCES

(1) Brust, M.; Bethell, D.; Kiely, C. J.; Schiffrin, D. J. Self-Assembled Gold Nanoparticle Thin Films with Nonmetallic Optical and Electronic Properties. *Langmuir* **1998**, *14*, 5425−5429.

(2) Freeman, R. G.; Grabar, K. C.; Allison, K. J.; Bright, R. M.; Davis, J. A.; Guthrie, A. P.; Hommer, M. B.; Jackson, M. A.; Smith, P. C.; Walter, D. G.; Natan, M. J. Self-Assembled Metal Colloid Monolayers: An Approach to SERS Substrates. *Science* **1995**, *267*, 1629.

(3) Zhao, J.; Bradbury, C. R.; Huclova, S.; Potapova, I.; Carrara, M.; Fermín, D. J. Nanoparticle-mediated electron transfer across ultrathin self-assembled films. *J. Phys. Chem. B* **2005**, *109*, 22985−22994.

DOI: 10.1021/acs.langmuir.9b00280
Langmuir 2019, 35, 6297−6303

(4) Kissling, G. P.; Miles, D. O.; Fermín, D. J. Electrochemical charge transfer mediated by metal nanoparticles and quantum dots. *Phys. Chem. Chem. Phys.* **2011**, *13*, 21175−21185.
(5) Bradbury, C. R.; Zhao, J.; Fermín, D. J. Distance-independent charge-transfer resistance at gold electrodes modified by thiol monolayers and metal nanoparticles. *J. Phys. Chem. C* **2008**, *112*, 10153−10160.
(6) Dyne, J.; Lin, Y. S.; Lai, L. M. H.; Ginges, J. Z.; Luais, E.; Peterson, J. R.; Goon, I. Y.; Amal, R.; Gooding, J. J. Some more observations on the unique electrochemical properties of electrode-monolayer-nanoparticle constructs. *ChemPhysChem* **2010**, *11*, 2807−2813.
(7) Barfidokht, A.; Ciampi, S.; Luais, E.; Darwish, N.; Gooding, J. J. Distance-dependent electron transfer at passivated electrodes decorated by gold nanoparticles. *Anal. Chem.* **2013**, *85*, 1073−1080.
(8) Le Saux, G.; Ciampi, S.; Gaus, K.; Gooding, J. J. Electrochemical Behavior of Gold Colloidal Alkyl Modified Silicon Surfaces. *ACS Appl. Mater. Interfaces* **2009**, *1*, 2477−2483.
(9) Liu, J.; Gooding, J. J.; Paddon-Row, M. N. Unusually rapid heterogeneous electron transfer through a saturated bridge 18 bonds in length. *Chem. Commun.* **2005**, 631−633.
(10) Young, S. L.; Kellon, J. E.; Hutchison, J. E. Small Gold Nanoparticles Interfaced to Electrodes through Molecular Linkers: A Platform to Enhance Electron Transfer and Increase Electrochemically Active Surface Area. *J. Am. Chem. Soc.* **2016**, *138*, 13975−13984.
(11) Razzaq, H.; Qureshi, R.; Schiffrin, D. J. Enhanced rate of electron transfer across gold nanoparticle-anthraquinone hybrids. *Electrochem. Commun.* **2014**, *39*, 9−11.
(12) Jensen, P. S.; Chi, Q.; Grumsen, F. B.; Abad, J. M.; Horsewell, A.; Schiffrin, D. J.; Ulstrup, J. Gold Nanoparticle Assisted Assembly of a Heme Protein for Enhancement of Long-Range Interfacial Electron Transfer. *J. Phys. Chem. C* **2007**, *111*, 6124−6132.
(13) Schiffrin, D. J. Current topics in physical and nanoparticle electrochemistry. *Curr. Opin. Electrochem.* **2017**, *4*, 112−117.
(14) Laviron, E. General expression of the linear potential sweep voltammogram in the case of diffusionless electrochemical systems. *J. Electroanal. Chem. Interfacial Electrochem.* **1979**, *101*, 19−28.
(15) Laviron, E. The use of linear potential sweep voltammetry and of a.c. voltammetry for the study of the surface electrochemical reaction of strongly adsorbed systems and of redox modified electrodes. *J. Electroanal. Chem. Interfacial Electrochem.* **1979**, *100*, 263−270.
(16) Liu, F.; Khan, K.; Liang, J. H.; Yan, J. W.; Wu, D. Y.; Mao, B. W.; Jensen, P. S.; Zhang, J.; Ulstrup, J. On the hopping efficiency of nanoparticles in the electron transfer across self-assembled monolayers. *ChemPhysChem* **2013**, *14*, 952−957.
(17) Chazalviel, J. N.; Allongue, P. On the origin of the efficient nanoparticle mediated electron transfer across a self-assembled monolayer. *J. Am. Chem. Soc.* **2011**, *133*, 762−764.
(18) Hill, C. M.; Kim, J.; Bard, A. J. Electrochemistry at a Metal Nanoparticle on a Tunneling Film: A Steady-State Model of Current Densities at a Tunneling Ultramicroelectrode. *J. Am. Chem. Soc.* **2015**, *137*, 11321−11326.
(19) Ostojic, N.; Thorpe, J. H.; Crooks, R. M. Electron Transfer Facilitated by Dendrimer-Encapsulated Pt Nanoparticles Across Ultrathin, Insulating Oxide Films. *J. Am. Chem. Soc.* **2016**, *138*, 6829−6837.
(20) Herrera, S.; Adam, C.; Ricci, A.; Calvo, E. J. Electrochemical gating of single osmium molecules tethered to Au surfaces. *J. Solid State Electrochem.* **2016**, *20*, 957−967.
(21) Creager, S. E.; Wooster, T. T. A New Way of Using ac Voltammetry To Study Redox Kinetics in Electroactive Monolayers. *Anal. Chem.* **1998**, *70*, 4257−4263.
(22) Ricci, A. M.; Calvo, E. J.; Martin, S.; Nichols, R. J. Electrochemical Scanning Tunneling Spectroscopy of Redox-Active Molecules Bound by Au−C Bonds. *J. Am. Chem. Soc.* **2010**, *132*, 2494−2495.
(23) Danilowicz, C.; Corton, E.; Battaglini, F. Osmium complexes bearing functional groups: building blocks for integrated chemical systems. *J. Electroanal. Chem.* **1998**, *445*, 89.
(24) Frens, G. Controlled Nucleation for the Regulation of the Particle Size in Monodisperse Gold Suspensions. *Nat. Phys. Sci.* **1973**, *241*, 20.
(25) Li, J.; Schuler, K.; Creager, S. E. Generalized equivalent-circuit model for electroactive monolayers exhibiting a fixed redox potential and a distribution of electron-transfer rate constants. I. Square distributions. *J. Electrochem. Soc.* **2000**, *147*, 4584−4588.
(26) Davia, F.; Herrera, S. E.; Calvo, E. J. Gaussian Distribution of Electron Transfer Distance in Redox Terminated Self-Assembled Thiol Monolayers. *J. Phys Chem. C* **2019** (submitted).
(27) Albery, W. J.; Bartlett, P. N.; Wilde, C. P.; Darwent, J. R. A general model for dispersed kinetics in heterogeneous systems. *J. Am. Chem. Soc.* **1985**, *107*, 1854−1858.
(28) Albery, W. J.; Boutelle, M. G.; Colby, P. J.; Hillman, A. R. The kinetics of electron transfer in the thionine-coated electrode. *J. Electroanal. Chem. Interfacial Electrochem.* **1982**, *133*, 135−145.
(29) Nahir, T. M.; Clark, R. A.; Bowden, E. F. Linear-Sweep Voltammetry of Irreversible Electron Transfer in Surface-Confined Species Using the Marcus Theory. *Anal. Chem.* **1994**, *66*, 2595−2598.
(30) Sabatani, E.; Anson, F. C. Mediated electron transfer across Nafion|solution interfaces. Comparison with Marcus theory for cases involving Gaussian arrays of mediator couples. *J. Electroanal. Chem.* **1995**, *386*, 111−119.
(31) Marmisollé, W. A.; Capdevila, D. A.; de la Llave, E.; Williams, F. J.; Murgida, D. H. Self-Assembled Monolayers of NH2-Terminated Thiolates: Order, pKa, and Specific Adsorption. *Langmuir* **2013**, *29*, 5351−5359.
(32) Bradbury, C. R.; Kuster, L.; Fermín, D. J. Electrochemical reactivity of HOPG electrodes modified by ultrathin films and two-dimensional arrays of metal nanoparticles. *J. Electroanal. Chem.* **2010**, *646*, 114−123.
(33) Shein, J. B.; Lai, L. M. H.; Eggers, P. K.; Paddon-Row, M. N.; Gooding, J. J. Formation of efficient electron transfer pathways by adsorbing gold nanoparticles to self-assembled monolayer modified electrodes. *Langmuir* **2009**, *25*, 11121−11128.
(34) De La Llave, E.; Herrera, S. E.; Adam, C.; Méndez De Leo, L. P.; Calvo, E. J.; Williams, F. J. Molecular and electronic structure of osmium complexes confined to Au(111) surfaces using a self-assembled molecular bridge. *J. Chem. Phys.* **2015**, *143*, No. 184703.
(35) Miller, C. J. In *Physical Electrochemistry*; Rubinstein, I., Ed.; Marcel Dekker: New York, 1995.

DOI: 10.1021/acs.langmuir.9b00280
Langmuir 2019, 35, 6297−6303